Advances in Science and Technology Research Journal

Advances in Science and Technology Research Journal, 2026, 20(5), 1–17
https://doi.org/10.12913/22998624/214846
ISSN 2299-8624, License CC-BY 4.0

Received: 2025.07.21
Accepted: 2026.03.15
Published: 2026.04.01

Rapid prototyping of optical lenses using the Isolation forest model for anomaly detection

Sylwester Tomasz Korga[1]

[1] Department of Computer Science, Faculty of Electrical Engineering and Computer Science, Lublin University of Technology, ul. Nadbystrzycka 38, Lublin, Poland
E-mail: s.korga@pollub.pl

ABSTRACT

The article presents the application of 3D printing technology in the production of optical lenses, which are used in fields such as mechanical engineering, computer science, and precision optics. The aim of the study was to design, manufacture, and verify the properties of transparent optical lenses made from photopolymer resins. The lenses were fabricated using stereolithography (SLA), a high-precision 3D printing method. The production process is described in detail, including the use of proprietary finishing tools that ensure precise lens processing crucial for achieving optimal optical properties. After printing, the lenses underwent finishing treatments including grinding, polishing, and UV curing, which significantly improved their optical quality. The best lenses demonstrated stable and high light transmission over a wavelength range from 380 to 1146 nm, with transmission values exceeding 90–92%. The optical properties of the lenses were assessed in a professional laboratory using a monochromator, allowing precise measurement and objective quality evaluation. A novel aspect of the study was the use of artificial intelligence in quality control. The Isolation Forest model was employed to detect anomalies in the optical transmission data, identifying 79 anomalies under incandescent light and 81 under xenon light, approximately 5% of the dataset. To better interpret the detected anomalies, SHapley Additive exPlanations (SHAP) were used to understand which features most influenced anomaly classification. Combining advanced 3D printing technology with AI-driven anomaly detection represents an innovative and promising approach to optical lens manufacturing. This integration enhances defect detection, enabling more effective quality assessment and optimization of the production process. This method offers significant potential for rapid prototyping in precision optics applications.

Keywords: lenses, rapid prototyping, additive manufacturing, Izolation Forest, Shap, anomaly.

INTRODUCTION

3D printing technology, also known as additive manufacturing, has revolutionized numerous fields of science and industry in recent years, enabling the rapid and cost-effective production of complex components with non-standard shapes. One area in which 3D printing is finding increasingly widespread application is optics—particularly in the rapid prototyping of lenses and other optical elements. Traditional methods for manufacturing lenses, such as grinding and polishing glass or injection molding of polymers, are time-consuming, expensive, and require specialized tooling [1]. The introduction of 3D printing technology has opened new possibilities in the areas of customization, iterative design, and rapid prototyping of optical components at relatively low cost. An optical lens can be defined as a device capable of transmitting and refracting light passing through it [2]. Lenses can be manufactured from glass, polymeric materials, or potentially any other material possessing suitable optical properties. A lens is constructed in such a way as to enable the formation of either reduced or magnified images. The primary functions of lenses are to focus or disperse light. This allows for the magnification or reduction of images. Differences in the curvature of lens surfaces affect their ability to refract light in a specific manner, tailored

to particular requirements and applications [3]. The primary area of application for optical lenses is ophthalmology. However, lenses are also used in various optical instruments, such as projectors, sensors, and lighting systems [4]. In manufacturing markets, there is a growing demand for production as well as a need for further technological development in the field of image processing methods utilizing optical components. The microlenses designed by the authors for lab-on-a-chip devices may prove useful in the production of devices such as three-dimensional displays, solar cells, photodetectors, or fiber optic systems [5–6]. In publication [7], the manufacturing process of lenses made from transparent photosensitive resins using SLA technology is presented. These lenses are used as coatings for high-power white light-emitting diodes (WLEDs). In order to achieve the desired and uniform direction of illumination as well as collimation, research has been initiated into alternative methods for lens fabrication. In the literature [8,9], the authors highlight the drawbacks of conventional lens manufacturing methods, which are associated with a high degree of production complexity, long production cycles, and high material costs. The increasing prevalence of 3D printing has led to significant changes in the approach to lens manufacturing, offering the possibility of faster prototyping, cost reduction, simplified assembly, and greater design flexibility. Lenses produced using 3D printing technology can be applied in many industries, such as optics, metrology, machine construction, automotive, and aviation [10–11]. Despite the growing popularity of 3D printing technology in the production of optical lenses, especially using the SLA method, quality control and defect detection remain challenges due to the complexity of processes and subtle material flaws. Current quality control methods are often time-consuming and unsuitable for rapid prototyping. The introduction of artificial intelligence models, such as Isolation Forest, for automatic anomaly detection at early stages of production is an innovative approach that can significantly optimize the process and improve product quality. This work fills this gap by demonstrating the possibility of combining the 3D printing process using SLA with defect detection through a classical AI algorithm, opening new opportunities for the fast and economical production of high-quality optical lenses.

In the lens manufacturing market, there are various types of 3D printing technologies, such as FDM, SLS, DLP, and PolyJet. However, according to information provided in the literature, stereolithography (SLA) is currently regarded as the most promising method for the fabrication of optical lenses [12–14]. The SLA technology enables the achievement of very high precision, surface smoothness, and print clarity, which are crucial for the production of optical components [15]. In study [16], the process of manufacturing and utilizing a proprietary resin curable with visible light is presented. Optical products fabricated using SLA technology from photopolymer resins are increasingly replacing expensive commercial products due to their excellent optical properties and the ability to dye the resin during its preparation. This allows for precise adjustment of material parameters to specific applications while simultaneously reducing production costs [17–19].

The authors of article [20] note that, in terms of stability and surface roughness, optical elements made of glass serve as the reference material for all polymer lenses. To assess quality, the authors compared spherical microlenses with diameters of 1 mm and 2 mm to readily available glass equivalents from Edmund Optics. The 3D printing technique offers greater design flexibility and lower manufacturing costs. However, direct comparison of glass and polymer optical microcomponents can be problematic, especially in the case of hard-to-obtain aspherical glass lenses with a diameter of 1 mm. The production of polymer lenses using 3D printing involves numerous technological and material challenges. Rapid prototyping of optical components by means of 3D printing is associated with a range of technological difficulties. The most important of these concern achieving the appropriate optical properties of the printed lenses, such as high transparency, optical homogeneity, and precise shape reproduction. During the printing process, defects such as layer boundaries, air bubbles, or microcracks may occur, which can significantly reduce the optical quality of the lenses [21]. Therefore, the selection of photopolymer resins with optical properties comparable to those of traditional polymers remains an important issue, as currently available materials often do not fully meet optical standards and require further research. The production of lenses most commonly involves the use of photopolymer resins or thermoplastic polymers, which must meet stringent requirements regarding light transmission, chemical and mechanical stability, and compatibility with the printing process [22].

Additionally, printed lenses require time-consuming and precise surface finishing processes, such as polishing or coating, to achieve the necessary smoothness and transparency. The lens production process should be optimized to reduce material waste and ensure proper disposal, including special disposal methods for certain materials. The lack of standardization in 3D printing technology and finishing process automation complicates the implementation of mass production, while the certification process for new materials and technologies according to ISO and FDA standards is lengthy and costly [23].

MATERIALS AND METHODS

Materials

In the rapid prototyping of optical lenses using 3D printing technology, the proper selection of materials and a thorough understanding of their optical and technological properties are of key importance. The scientific literature describes a variety of materials used for the fabrication of optical components by means of 3D printing [24–26]. However, in additive 3D printing technology, photopolymer resins cured with light of a strictly defined wavelength are most commonly used [27]. Therefore, photopolymer resins were selected for the lens manufacturing process using 3D printing technology due to their properties that enable the production of high-quality optical components. Photopolymer resins exhibit a wide range of mechanical properties—from flexible to very rigid—high transparency, and the possibility of further finishing processes such as grinding or polishing. Their composition includes monomers and oligomers, photoinitiators, and additives that modify mechanical and optical properties [28]. 3D-printed lenses must meet stringent optical, dimensional, and mechanical requirements. One of the main technological challenges is the anisotropy of optical properties, manifested as varying transparency and strength depending on the printing direction. In the Z axis, perpendicular to the layers, increased light scattering is observed at interlayer boundaries, while in the X/Y axes it is possible to achieve acceptable optical homogeneity. Another important technological feature is low surface roughness (Ra < 20 nm), which limits light scattering. High transparency is defined as light transmission above 92% in the 400–700 nm range. Dimensional accuracy is also essential, with tolerances at the level of ±0.05 mm for lenses with a diameter of approximately 50 mm [29]. Despite using manufacturer-recommended 3D printing parameters, the lens fabrication process still promotes the formation of structural defects. The most common include air bubbles formed during resin curing, microcracks resulting from thermal or mechanical stresses, and chemical inhomogeneities caused by incomplete polymerization [30].

Methodology of the study

Prototyping of lens models

The design of lenses is a complex process in which precise technological requirements and

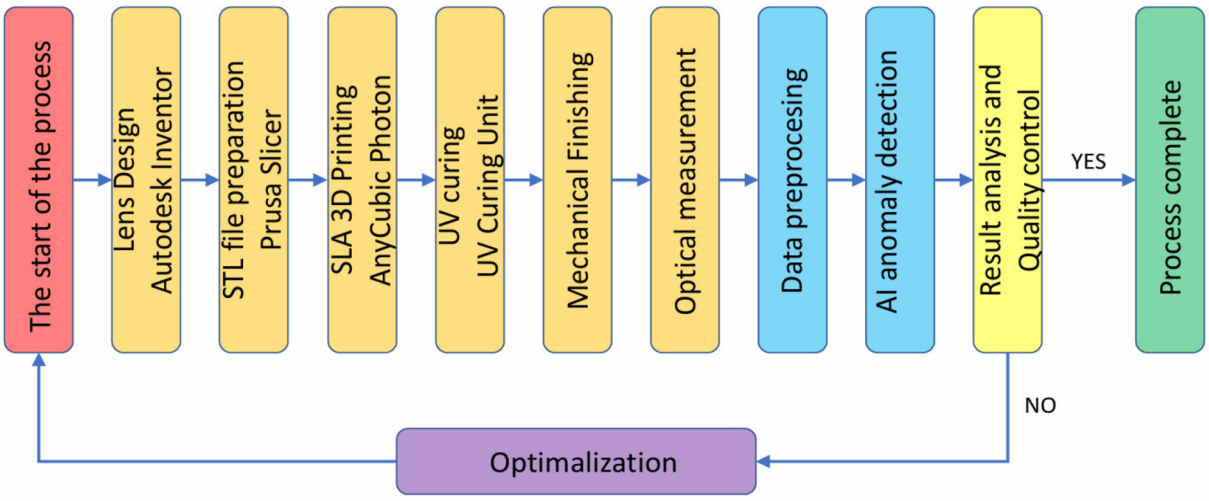

Figure 1. Block diagram of the rapid prototyping process for optical lenses using 3D printing and AI-based anomaly detection

unambiguous communication between the designer and manufacturer play a key role. This is a multi-stage process in which various technological operations are carried out at each stage. The sequence diagram of the manufacturing process – from design to the final product – is presented in Figure 1.

In the lens design process, the ISO 10110 series of standards is of particular importance, as it standardizes the way in which the quality parameters of optical components are described on technical drawings. This standard covers a wide range of issues, such as material requirements, shape and position tolerances, surface quality, permissible material defects (e.g., inclusions, bubbles, stresses), centering tolerances, and specifications for optical coatings. Each of these parameters-including radius of curvature, thickness, diameter, surface roughness, and the number and size of defects – should be clearly defined according to the relevant part of the standard and precisely recorded in the design documentation. The use of ISO 10110 ensures effective information exchange within international engineering teams, minimizes the risk of interpretational errors, and guarantees that the finished lens will meet both optical and mechanical requirements [31]. The lens models intended for research were prepared in accordance with the ISO 10110 standard. Autodesk Inventor 2024 software was used to design the models. The set of lens models is shown in Figure 2. The solid model files were saved in STL format and imported into PrusaSlicer software version 2.3. Instead of using support structures, edge rounding was applied at the points where the products contact the build plate. This solution facilitated the removal of the prints from the platform and proved effective in the case of plano-convex lenses.

The process of manufacturing lenses using SLA technology

Selected resin materials were chosen based on the optical properties declared by their manufacturers, such as high transparency, high product strength, and compatibility with the 3D printer used for production – AnyCubic Photon Mono (see Figure 3). The first series of lenses was made from AnyCubic Clear resin. Samples from this series were labeled with the letter A. This is a transparent resin dedicated to AnyCubic Photon SLA printers, featuring increased strength during the curing process. The second series of samples was made from 3DM-Tough resin. Samples from this series were labeled with the letter T. This is a transparent resin with enhanced mechanical strength, containing

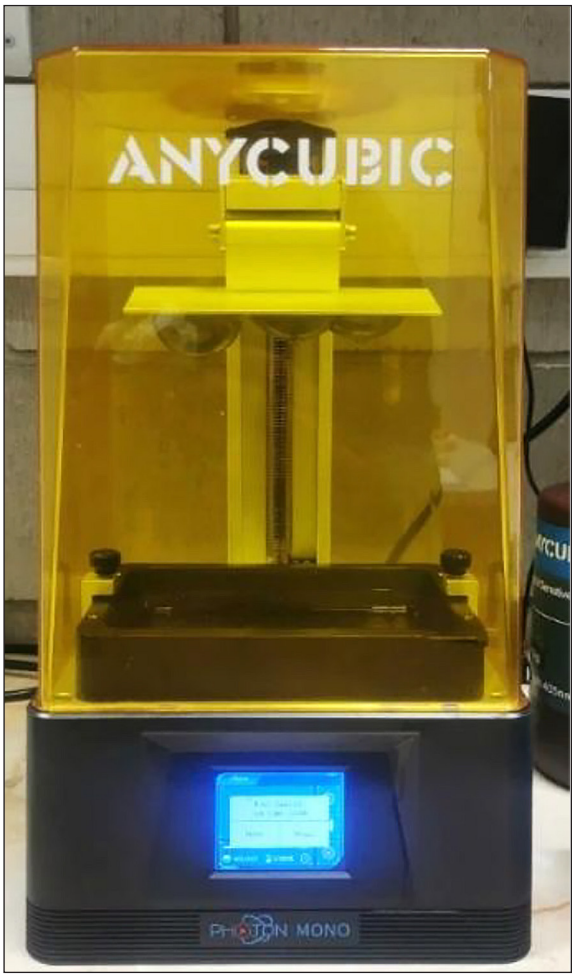

Figure 3. AnyCubic Photon Mono SLA 3D printer with visible printed lenses

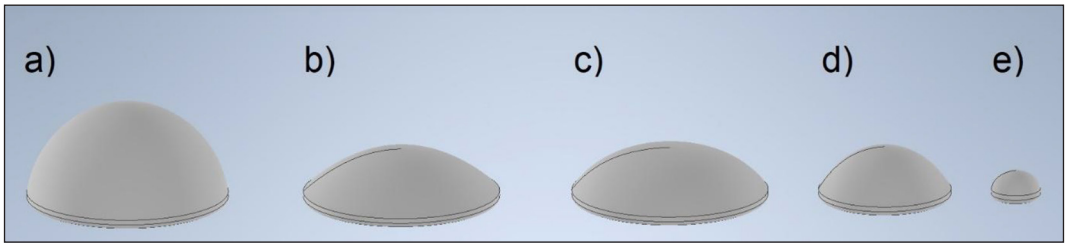

Figure 2. View of lens models: (a) L1A/L1T, (b) L2A/L2T, (c) L3A/L3T (d) L4A/L4T (e) L5A/L5T

an additive of blue dye that stabilizes the color of the products. Both resins are intended for curing with UV light at a wavelength of 405 nm. Table 1 presents a comparison of the material properties of AnyCubic high clear and 3DM-Tough resins

The technological parameters for manufacturing the lenses were based on the knowledge presented in the work [32], which is a recognized and proven method in the technology of SLA 3D printing of optical resins. This method guarantees high optical quality and printing precision, confirming its effectiveness and correctness in producing advanced microscopic components.

The AnyCubic Photon 3D printer utilizes a monochromatic LCD matrix with a 6-inch diagonal and a resolution of 2560 × 1620 pixels during its operation cycle. The printing accuracy in the Z-axis varies, allowing for a single layer height ranging from 0.01 to 0.15 mm. The maximum achievable print speed is 50 mm/h, and the exposure time for a single layer ranges from 1.5 to 2 seconds. The AnyCubic Photon printer performs the printing process using Bottom-Up SLA technology, which is a better choice for producing lenses sized from 10 mm to 40 mm than the Top-Down technology. The selected 3D printing parameters were consulted with industry specialists from the Prolight laboratory. To compare the obtained products, it was decided to apply uniform technological parameters for the production of each set. Due to the capability of printing multiple elements simultaneously, the process of printing 5 lenses concurrently was chosen. The layer height was set to 0.05 mm, which is recommended in the printer's technical documentation. Because support structures were not used in the sets, appropriate initial layers ensuring sufficient adhesion to the substrate had to be made. The number of base layers was 25, with an exposure time of 15 seconds. Subsequent layers were exposed every 9 seconds. Efforts were made to select parameter values to achieve an isotropic structure of the product throughout its volume. The sets of printed lenses are shown in Figures 4 and 5.

Both sets of lenses printed using the SLA method exhibited surface roughness and opacity, which prevented their use in optical systems. To achieve the required transparency and surface smoothness, it was decided to apply specialized post-processing techniques, including grinding and polishing with the use of polishing pastes.

Post-processing of polymeric lenses

The sets of lenses printed using SLA technology were subjected to final curing in a DWS UV

Table 1. Comparison table of material properties for AnyCubic high clear and 3DM-tough resins

Property	AnyCubic high clear resin	3DM-tough resin
Transparency	Very high, crystal clear	High, slightly less clear
Mechanical strength	Moderate toughness	High toughness and durability
Hardness (Shore D)	Approx. 78 D	84–86 D
Tensile strength	~28 MPa	50–60 MPa
Elongation at break	~14.6%	5–7%
Flexural strength	~30 MPa	60–70 MPa
Flexural modulus	~800 MPa	2000–2200 MPa
Viscosity	~266 cP	110–130 mPa·s
UV cure wavelength	365–405 nm	365–405 nm
Typical applications	Transparent prototypes	Transparent prototypes

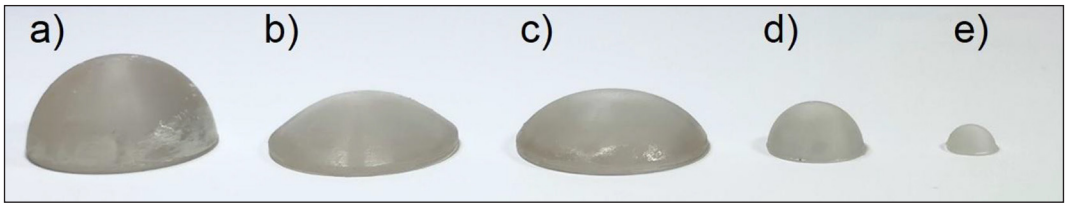

Figure 4. A set of lenses fabricated from AnyCubic resin before finishing treatment: (a) L1A/S1T, (b) L2A/L2T, (c) L3A/L3T, (d) L4A/L4T, (e) L5A/L5T

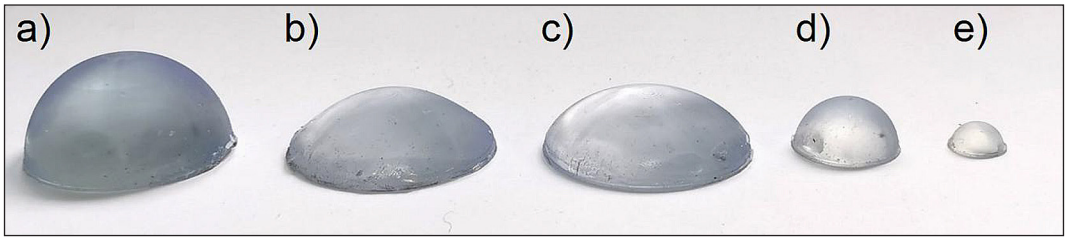

Figure 5. A set of lenses fabricated from 3DM-Tough resin before finishing treatment: (a) L1A/L1T, (b) L2A/L2T, (c) L3A/L3T, (d) L4A/L4T, (e) L5A/L5T

Curing Unit by exposure to ultraviolet radiation (see Figure 6). The post-cure process enabled complete polymerization of the photopolymer material, which resulted in increased mechanical strength and chemical stability of the prints. Additional UV curing also improved the surface properties of the models, such as smoothness and the precision of detail reproduction, while simultaneously eliminating the residual tackiness left after printing.

The post-processing steps, including precise polishing and surface finishing of the lenses, were conducted according to established protocols described in work [33]. It is pointed out there that accurate surface treatment is essential to achieve high optical transparency and reduction of surface imperfections caused by 3D printing. Such finishing ensures optimal lens properties by enhancing clarity and reducing light scattering. After the exposure process, the lenses were characterized by numerous surface contaminants and scratches. In some cases, internal irregularities such as air bubbles and inclusions could be observed within the material structure. The appearance of selected lenses after the curing processes is shown in Figure 7 and Figure 8.

Lenses exhibited basic optical properties observable without the use of measuring equipment, i.e., the ability to observe the substrate at low magnification. To achieve transparency effects, each product required precise finishing treatment. The stereolithography process caused each lens to have visible boundaries in the top layer zone. Irregularities on the surfaces caused refraction, scattering, and diffraction of light. Therefore, abrasive processing was applied.

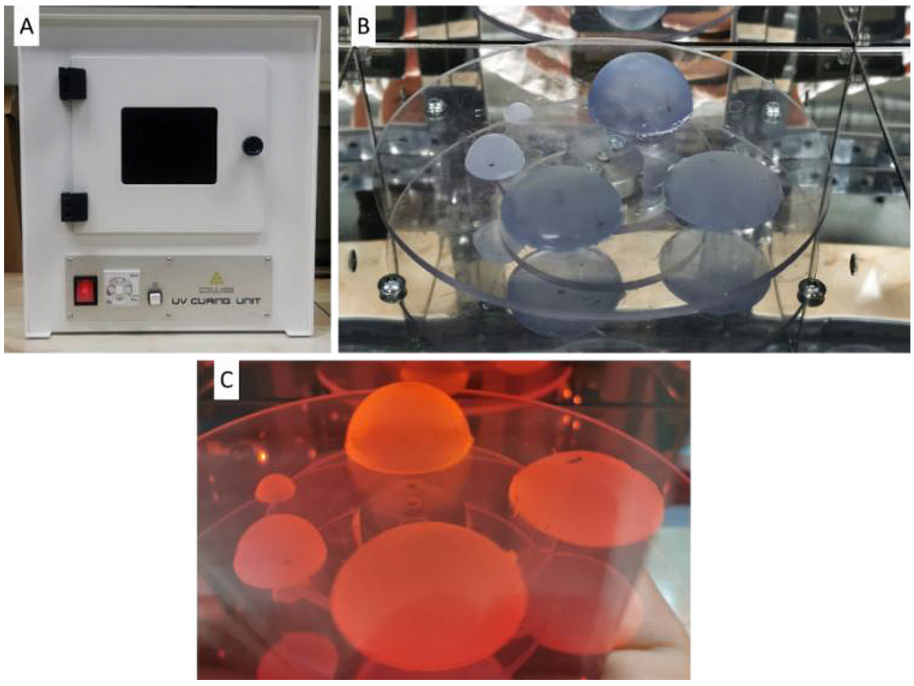

Figure 6. DWS UV illuminator: (a) view of the device, (b) view of the set of lenses made from 3DM-Tough resin placed in the device, (c) view of the lenses during UV light curing

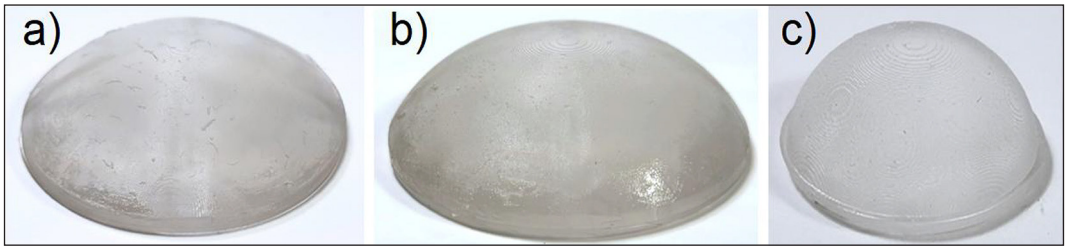

Figure 7. Lenses after the annealing process L2A, L3A, L5A

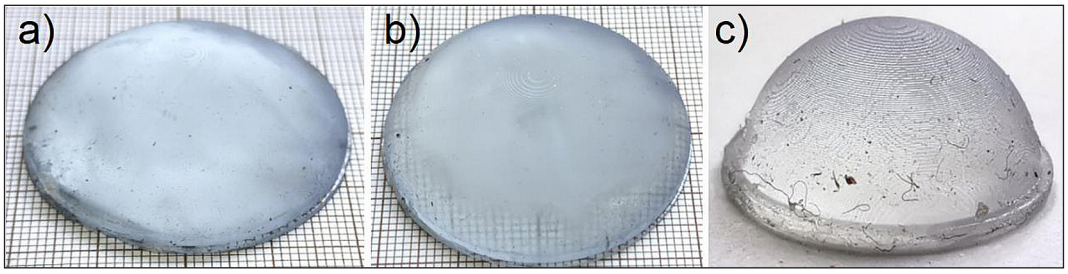

Figure 8. Lenses after the annealing process L2T, L3T, L5T

The abrasive processing of each lens involved wet sanding with sandpaper mounted in a special attachment. The rough processing of lenses began with the use of sandpapers with grits of 600 and 800. The finishing surface treatment started with sandpapers of grits 1000, 1200, 1500, 2000, 2500, 3000, and 5000. The abrasive processing was carried out using wet sandpapers. This allowed for continuous washing out of the abraded material residues and prevented their accumulation between the abrasive surface and the product surfaces. Precise sanding of the top layer was crucial for the success of the process to remove localized defects and scratches. For the polishing process of the lens surfaces, a polishing machine with a power of 270 W and speed regulation in the range of 800–12500 rpm was used, equipped with felt fiber tips. The rotational speed of the abrasive element did not exceed 1200 rpm. The polishing process was carried out using K2 Lamp Doctor paste intended for transparent polymer reflector surfaces. Tables 2 and 3 present and describe the methods and parameters of the finishing treatment for individual lenses. The total time required for precise finishing of the surface of one set of lenses was 3.5 hours.

Table 2. Dimensions of lenses made from AnyCubic resin before and after finishing treatment

AnyCubic		L1A		L2A		L3A		L4A		L5A	
		Semicircular lens		Parabolic lens		Elliptical lens		Semicircular lens		Semicircular lens	
Before finishing	No.	⌀ [mm]	H [mm]	⌀ [mm]	H [mm]	⌀ [mm]	H [mm]	⌀ [mm]	H [mm]	⌀ [mm]	H [mm]
	1	40.75	20.25	40.90	10.9	40.50	10.8	20.55	10.00	10.75	5.10
	2	40.9	20.00	40.90	10.86	40.50	10.75	20.45	10.00	10.70	5.15
	3	40.7	20.10	40.85	10.86	40.05	10.7	20.60	10.00	10.70	5.10
	Mean	40.78	20.11	40.88	10.87	40.35	10.75	20.53	10.00	10.71	5.11
After finishing	No.	⌀ [mm]	H [mm]	⌀ [mm]	H [mm]	⌀ [mm]	H [mm]	⌀ [mm]	H [mm]	⌀ [mm]	H [mm]
	1	40.60	19.50	40.60	10.50	40.05	10.60	20.14	9.70	9.80	4.86
	2	40.40	19.50	40.40	10.54	40.80	10.56	20.10	9.86	9.86	4.84
	3	40.60	19.56	40.40	10.50	40.82	10.58	20.14	9.80	9.90	4.86
	Mean	40.53	19.52	40.46	10.51	40.55	10.58	20.12	9.78	9.85	4.85
	Deviation from nominal dimension	0.53	0.48	0.46	0.51	0.55	0.58	0.12	0.22	0.15	0.15

Table 3. Dimensions of lenses made from 3DM-Tough resin before and after finishing treatment

3DM-Tough		L1T Semicircular lens		L2T Parabolic lens		L3T Elliptical lens		L4T Semicircular lens		L5T Semicircular lens	
Before finishing	No.	⌀ [mm]	H [mm]	⌀ [mm]	H [mm]	⌀ [mm]	H [mm]	⌀ [mm]	H [mm]	⌀ [mm]	H [mm]
	1	41.10	20.10	41.65	10.95	41.20	10.85	20.95	10.05	11.20	5.10
	2	41.25	20.15	42.10	10.95	41.60	10.85	21.25	10.05	11.15	5.10
	3	41.45	20.10	41.40	10.90	41.65	10.85	21.10	10.00	11.20	5.10
	Mean	41.26	20.12	41.71	10.93	41.38	10.85	21.10	10.03	11.18	5.10
After finishing	No.	⌀ [mm]	H [mm]	⌀ [mm]	H [mm]	⌀ [mm]	H [mm]	⌀ [mm]	H [mm]	⌀ [mm]	H [mm]
	1	40.08	20.02	40.75	10.35	40.75	10.10	20.20	9.65	9.90	4.40
	2	40.06	20.02	40.90	10.35	40.75	10.15	20.15	9.65	9.90	4.40
	3	40.08	20.02	40.80	10.35	40.75	10.10	20.00	9.65	9.85	4.40
	Mean	40.07	20.02	40.81	10.35	40.75	10.11	20.11	9.65	9.88	4.40
	Deviation from nominal dimension	0.73	0.02	0.81	0.35	0.75	0.11	0.11	0.35	0.12	0.6

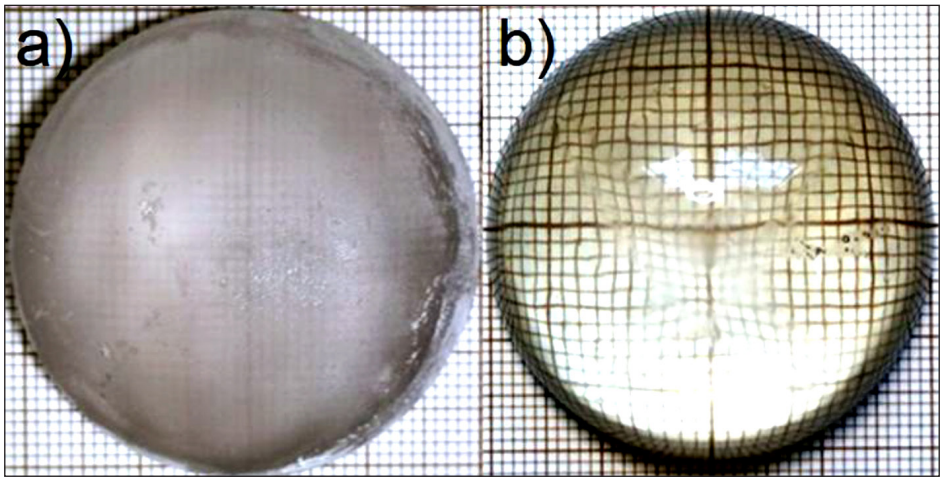

Figure 9. Lens L3A before treatment (a) and after treatment (b) – view of diagonal lines where uneven light refraction occurs

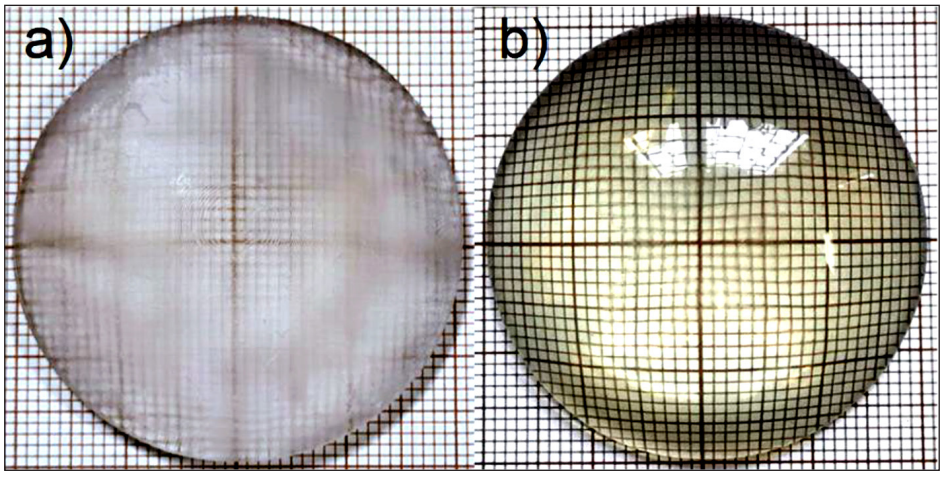

Figure 10. Lens L4A before (a) and after treatment (b). The view of the lines after treatment indicates improved transparency and optical surface quality of the lens

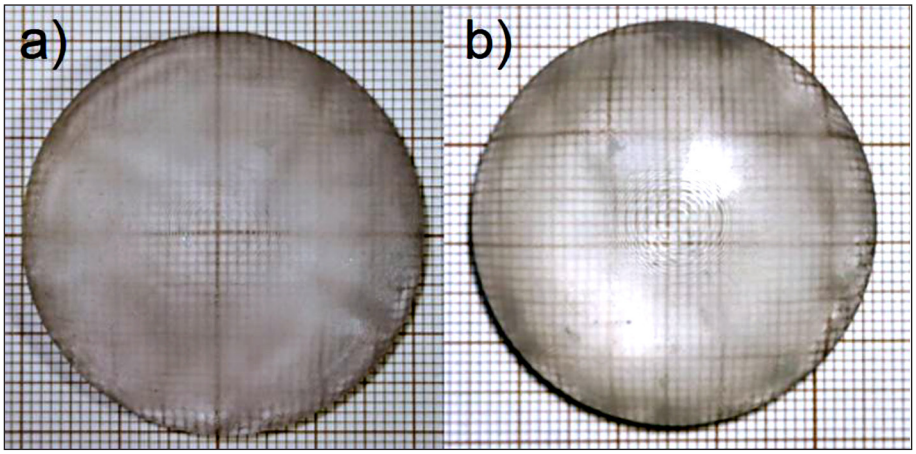

Figure 11. Lens L4A before (a) and after treatment (b). The view of the lines after treatment indicates improved transparency and optical surface quality of the lens

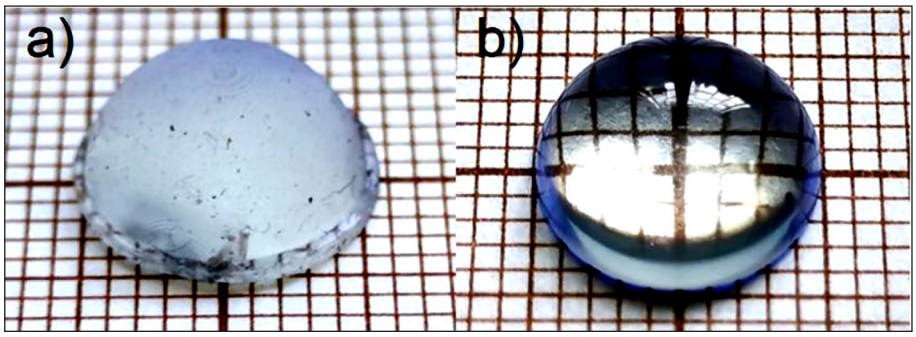

Figure 12. Lenses L3T before (a) and after the polishing process (b)

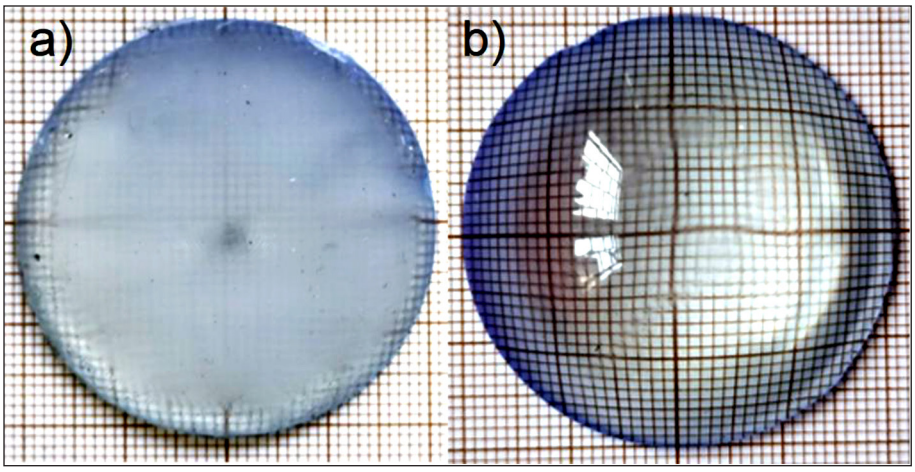

Figure 13. Lens L4T before (a) and after the polishing process (b)

RESULT AND DISCUSSION

Visual assessment of the obtained results

Figures 9 to 14 show the optical lenses before and after the grinding process. The presented photographs and descriptions illustrate how the surface of the lenses changed as a result of the abrasive treatment. This made it possible to perform a preliminary assessment of the effects of the applied finishing methods. Based on the presented photographs and descriptions, it can be clearly stated that the abrasive and polishing process significantly improved the surface quality of the optical lenses. The obtained results provide a basis for further analysis of the effectiveness of

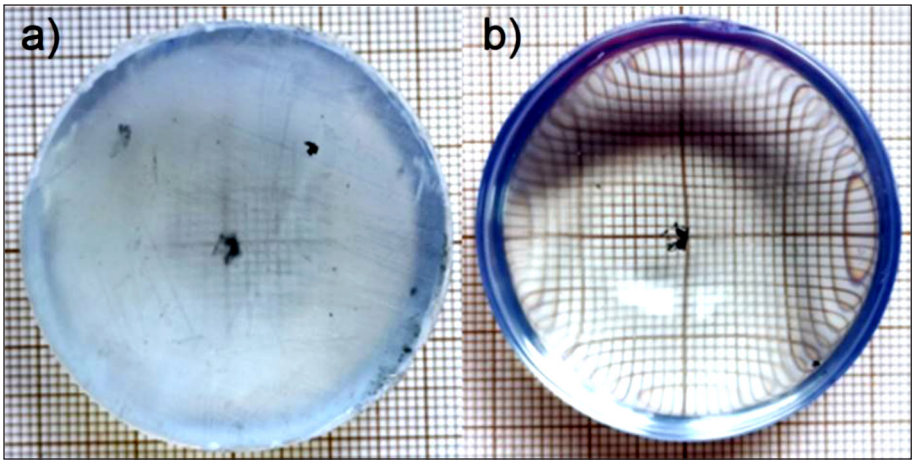

Figure 14. Lens L5T before (a), and after polishing process (b). Visible contamination inside the internal structure

the applied finishing methods in the context of their impact on the optical properties of the examined elements. Despite precise post-processing, optical lenses produced by 3D printing may still exhibit defects and anomalies such as internal air bubbles, surface scratches, or material inclusions, which adversely affect their optical performance. Detection and characterization of these imperfections are crucial to ensuring the high quality and functionality of the lenses. Therefore, appropriate validation methods must be employed in the production process. A promising approach proposed by the author is the use of artificial intelligence models to evaluate technological parameters. Such solutions are novel and still require further verification, as discussed in the literature [34].

Analysis of results

During the laboratory tests, detailed measurements of the optical properties of the prototype lenses were carried out, and the results are presented in graphs numbered 15 to 20. Each lens was tested for light transmission in the wavelength range from 380 nm to 1146 nm, using two types of light sources: incandescent (orange functions) and xenon (blue functions). The analysis of the graphs allowed for a comparison of the optical quality of individual samples finished by polishing with sandpapers of different grit sizes. Lens L3A (graph 15) is characterized by very uniform light transmission across the entire tested spectral range. For both the incandescent and xenon light sources, the graphs are flat, indicating high and stable light transmittance regardless of wavelength. This means that lens L3A provides the most uniform transmission and the highest optical quality among the analyzed samples. Very similar properties are exhibited by lens L3T (graph 16), whose transmission graphs are also very flat and stable throughout the entire wavelength range. Lenses L4A (graph 17) and L4T (graph 18) exhibit slightly greater fluctuations in light transmission, especially in the wavelength range from 400 to 700 nm. The graphs for these samples are less flat than in the case of S3A and S3T, which suggests lower uniformity of light transmittance. Nevertheless, the transmission values remain high, and the differences between the measurements for both light sources are relatively small, indicating good, though not perfect, optical quality of these lenses. Lenses L5A (graph 19) and L5T (graph 20) show the greatest deviations from the ideal transmission characteristics among the analyzed samples. There are clear drops in transmission in specific wavelength ranges, and the graphs are the least uniform. This may be the result of material defects or less effective finishing processes. The differences between the measurements for the incandescent and xenon light sources are more pronounced, which confirms the lower optical quality of these samples compared to lenses L3A and L3T (Figures 15–20).

Among all the analyzed lenses, the best optical properties were demonstrated by lenses S3A and S3T, whose transmission graphs are the flattest and show the smallest differences between measurements for different light sources. This means that these lenses provide the most uniform and highest light transmission across the entire tested wavelength range, which is crucial for applications requiring high optical quality.

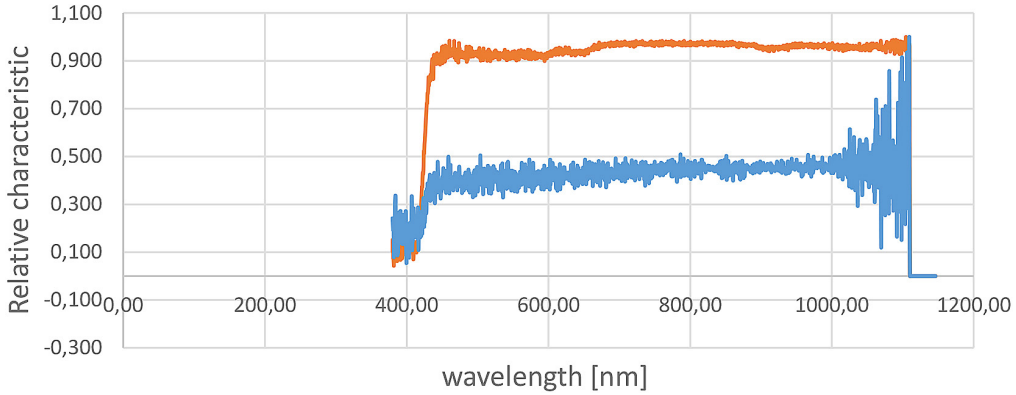

Figure 15. Relative characteristic of lens L3A

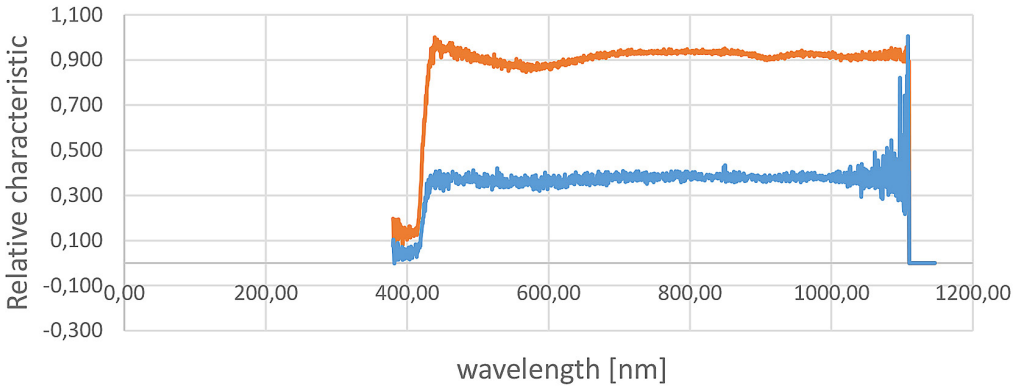

Figure 16. Relative characteristic of lens L3T

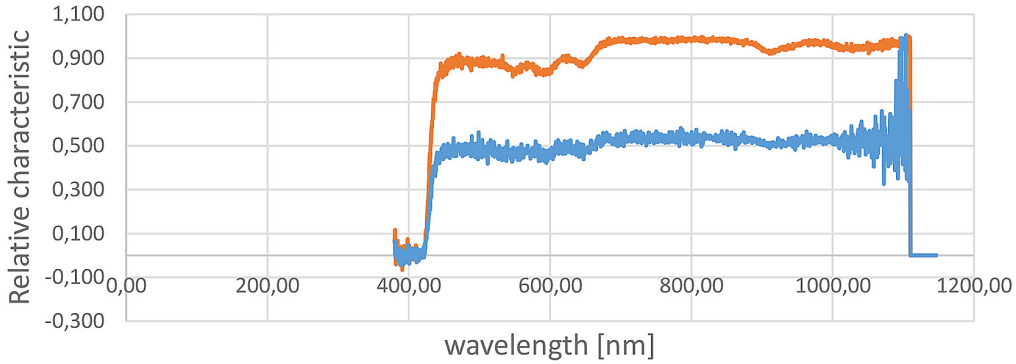

Figure 17. Relative characteristic of lens L4A

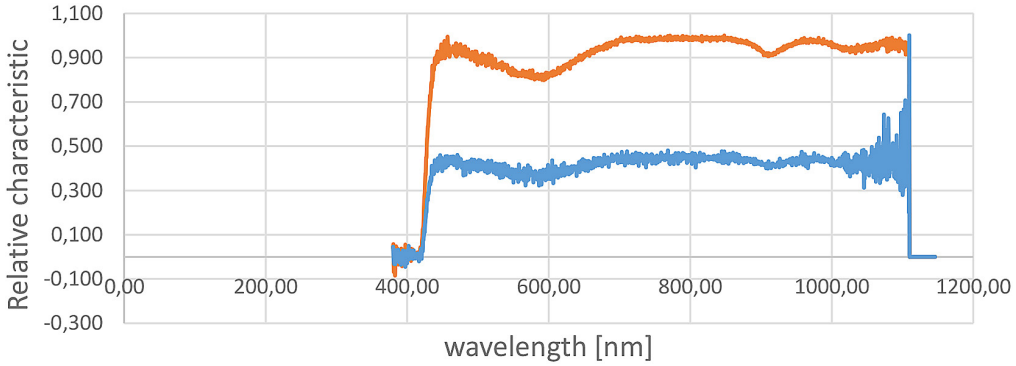

Figure 18. Relative characteristic of lens L4T

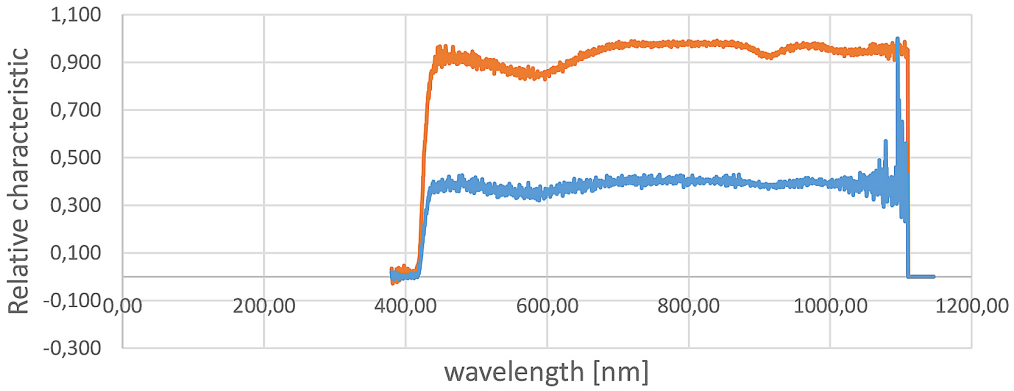

Figure 19. Relative characteristic of lens L5A

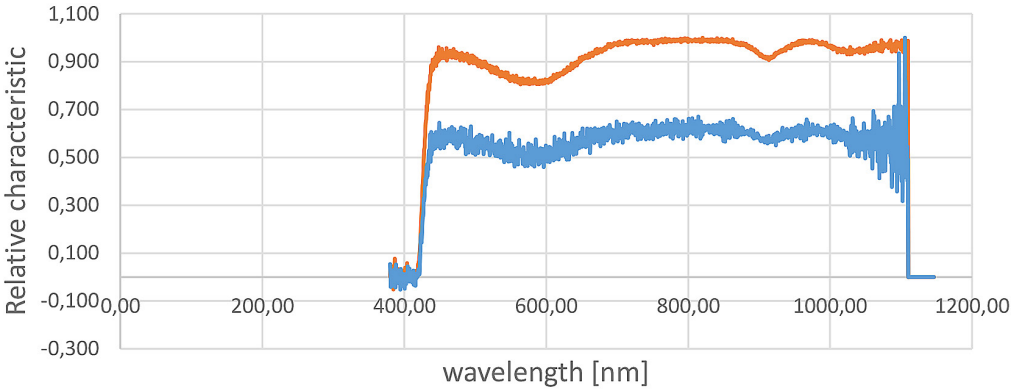

Figure 20. Relative characteristic of lens L5T

Lenses L4A and L4T exhibit moderate optical quality, while L5A and L5T are characterized by the greatest deviations and the lowest uniformity of transmission in this group.

AI research in anomaly detection for optical lenses

Scientific literature describes a wide range of artificial intelligence models applied for anomaly detection across various research domains. These models include both modern neural networks, such as convolutional neural networks (CNNs) used for raster image analysis, as well as classical methods based on computational algorithms for analyzing data sets [35]. To evaluate the applicability of AI in quality analysis of optical lenses, studies were conducted on a selected 20 mm spherical lens model (L4A). The analysis included measurement data obtained from incandescent and xenon light sources, enabling a comprehensive evaluation of their optical properties. Each data record has 5 dimensions (features) that describe various light transmission properties through the lens. For anomaly detection, the Isolation Forest model was chosen, being one of the most commonly used methods in scientific literature. This method relies on a computational algorithm that isolates outlier points through random data partitioning, allowing anomaly detection without explicitly modeling normal behavior. The Isolation Forest algorithm detects anomalies by isolating observations through random data partitions. It builds an ensemble of isolation trees, where each tree recursively splits data by randomly selecting features and split values. Anomalies are easier to isolate, resulting in shorter average path lengths in the trees, enabling effective identification.

For the study, lens L4A was selected because it exhibited instability in characteristics for incandescent and xenon light. The dataset saved in CSV format contained 1575 measurement points for both incandescent and xenon light.

The data underwent a preprocessing procedure which included:

- standardization of numerical value format,
- removing spaces,

- converting data from text format to numerical values,
- imputation, i.e., filling missing values with the mean value of the respective column.
- Only after such data cleansing was the model trained. The Isolation Forest model was imported from the sklearn.ensemble library. The following hyperparameters were chosen:
- n_estimators=100 – the number of decision trees forming the Isolation Forest, increasing anomaly detection accuracy at the cost of computation time,
- contamination=0.05 – the estimated percentage of anomalies in the data, influencing detection sensitivity,
- random_state=42 – setting the random seed to ensure reproducibility of results.

Models were trained separately for data with incandescent and xenon lighting. 79 anomaly points were detected for incandescent light and 81 for xenon light. The computation time on the test computer was approximately 48 seconds. For incandescent light, the CPU time (active processor time) measured was 62.5 ms and the real elapsed wall time was 59.3 ms; for xenon light, these values were 62.5 ms and 63 ms, respectively.

On charts 21 and 22, the results of anomaly detection for lens L4A are presented, obtained using the Isolation Forest model on two datasets: transmission under incandescent illumination (top chart) and xenon illumination (bottom chart). The X-axis represents the wavelength [nm], and the Y-axis shows the normalized transmission of radiation through the lens.

For both types of illumination, points classified as anomalies (red color) are concentrated at the beginning and end of the wavelength range, as well as in selected central segments of the

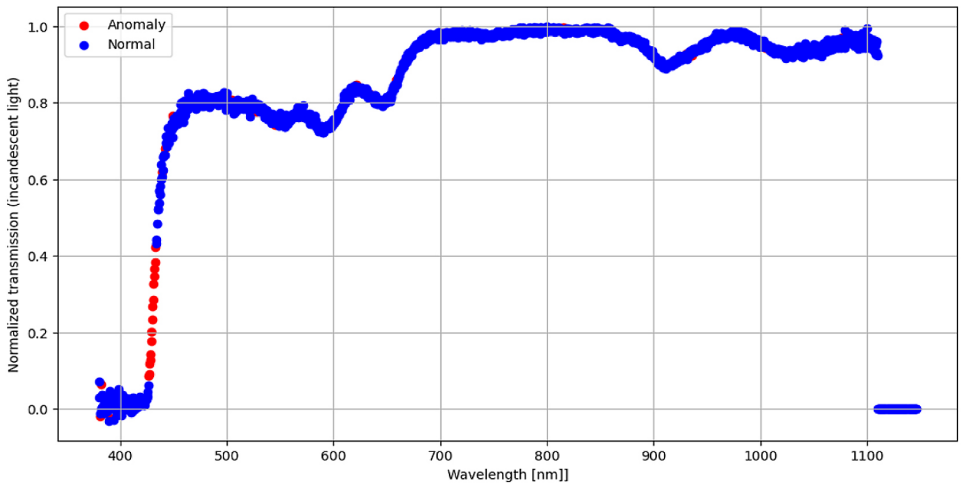

Figure 21. Anomaly detection using the Isolation Forest method for incandescent light data

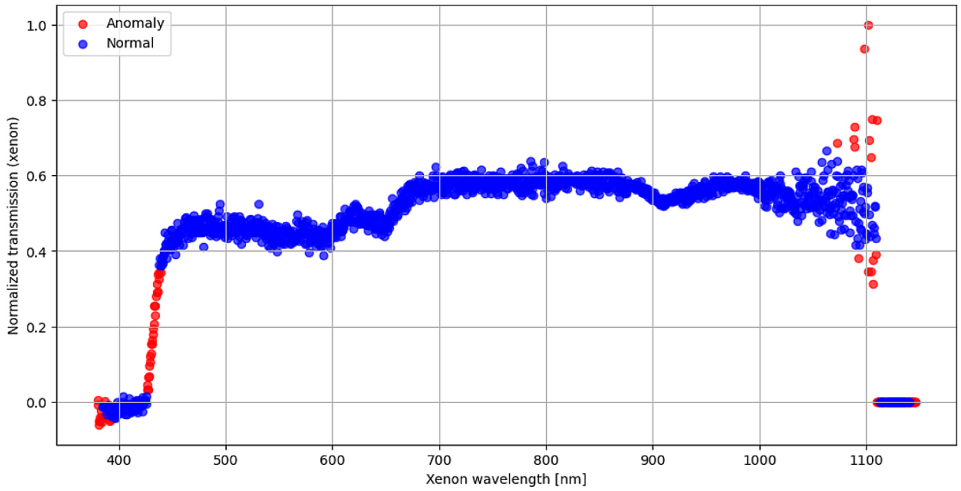

Figure 22. Anomaly detecting using the Isolation Forest method for xenon data

recording. The majority of measurements were classified as normal (blue color), which indicates a prevailing repeatability of transmission characteristics in the central part of the optical band. In the case of incandescent light, anomalies are mainly observed in regions where the transmission characteristic changes rapidly (e.g., the rising edge at short wavelengths and the drop at the end), which may correspond to areas with higher measurement noise levels or actual material instabilities. For xenon light, anomalies clearly appear at the spectrum boundaries and in the region above 1000 nm, where individual distant outlier points can be observed.

In the analysis of anomaly detection charts, it should be assumed that each red point on the plot represents an observation classified by the model as an anomaly, i.e., a deviation from the dominant pattern in the dataset. However, these marks do not always correspond to actual defects or damage of the lens – the Isolation Forest model identifies anomalies based on their isolation from the reference data cloud. In practice, outlier points may result from material instability, the presence of air bubbles, measurement errors, or local deviations in transmission caused by natural variability and measurement noise, especially at the extremes of the measurement range or in regions of abrupt spectral changes. Areas on the plots corresponding to sharp transitions or vertical characteristics can exhibit an increased number of detected anomalies; nevertheless, the interpretation of such results should be supported by expert knowledge and supplementary quality control methods. To further interpret the output of the anomaly detection process, the SHAP (SHapley Additive exPlanations) method was applied, enabling attribution of the model's predictions to specific measured features. Two SHAP summary plots were generated: one for the Bulb light configuration and one for the Xenon light configuration-Figure 23 and 24.

For the Bulb light setup, the SHAP summary plot (Figure 23) revealed that the features Differential_Characteristics_for_a_Light_Bulb and Normalized_to_max had the highest impact on the anomaly scores assigned by the Isolation Forest model. High values of Differential_Characteristics_for_a_Light_Bulb tended to increase the probability of classifying a measurement as an anomaly, whereas changes in Normalized_to_max could shift predictions in both directions, depending on the value. The influence of wavelength-related features was present but less pronounced.

For the Xenon light configuration, the SHAP summary plot (Figure 24) similarly indicated that Normalized_to_max and Differential_Characteristics_for_Xenon were the most influential variables for anomaly detection. The plot demonstrates that both high and low values of these features systematically affected the model's output, reflecting their key roles in distinguishing typical measurements from those flagged as outliers. The summary visualization offers insight into which measured transmission characteristics most directly inform the anomaly classification for each lighting scenario, highlighting the value of explainable AI in supporting optical quality control.

In future research, the plan is to develop dedicated artificial intelligence models better tailored to the specifics of measurements of lenses with confirmed defects, allowing precise

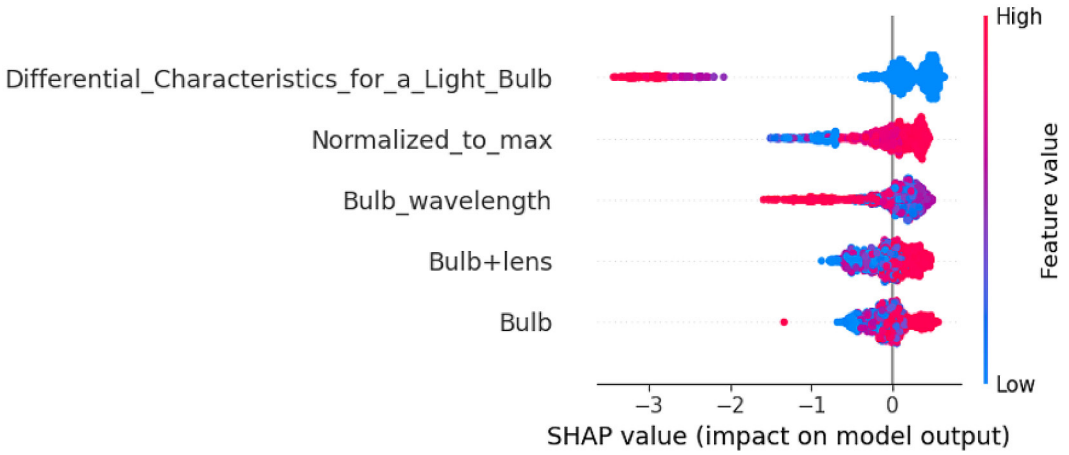

Figure 23. SHAP summary plot for bulb light measurements

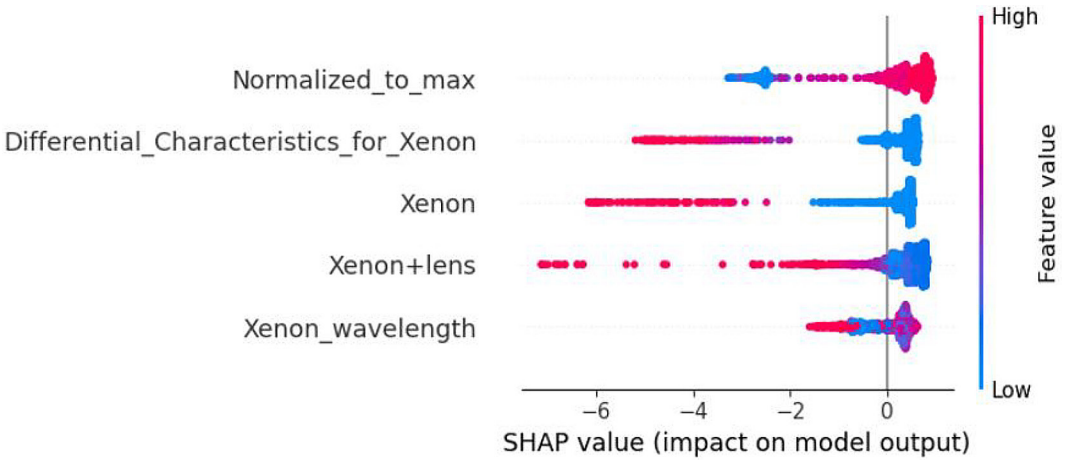

Figure 24. SHAP summary plot for xenon light measurements

determination of anomaly detection thresholds and optimization of quality control parameters. A key goal will be reducing false alarms through advanced validation and interpretation of results, including the use of explainable AI (XAI) techniques. Finally, the work will focus on automating the diagnosis of new lenses with unknown conditions by employing adaptive machine learning methods [36,37].

CONCLUSIONS

This article presents the possibilities and limitations of rapid prototyping of optical lenses using stereolithography (SLA) 3D printing technology. The conducted studies confirmed that polymer lenses with high transparency and favorable optical properties can be produced by using photopolymer resins coupled with appropriate finishing processes. The critical step in achieving high optical quality was the application of additional ultraviolet curing and precise mechanical finishing, including grinding and polishing. These processes effectively eliminated surface defects such as scratches and irregularities, which cause light scattering and diffraction. Spectral transmission analysis showed that lenses such as L3A and L3T exhibit the most uniform and stable light transmittance across a broad wavelength range, making them optimal candidates for applications requiring high optical quality. Polished lenses (e.g., L4A, L4T) demonstrated moderate quality, while lenses with material defects and less effective processing (e.g., L5A, L5T) exhibited significant deviations and lower transmission uniformity.

A significant part of the research involved the use of an artificial intelligence model, Isolation Forest, for automatic anomaly detection in optical measurement data. This model enabled the identification of outlier points that could correspond to defects or measurement noise. The application of SHapley Additive exPlanations (SHAP) further improved understanding of the features that most influence anomaly classification, thereby enhancing interpretability and providing insights into quality-related issues linked to materials and production processes.

Future research will develop specialized AI models aimed at detecting and characterizing lens defects, incorporating interpretability offered by explainable AI (XAI) techniques. The goal is to optimize anomaly detection thresholds and reduce false alarms, facilitating improved quality control and more reliable automation of diagnostics for lenses with unknown production states.

In summary, the integration of advanced AI methods with SLA printing technology and finishing processes represents a promising approach for cost-effective production and quality control of high-performance optical lenses. The author would like to express sincere gratitude to PhD Jacek Kęsik for his invaluable substantive support and practical assistance in the process of lens 3D printing. Special thanks are also extended to the Prolite Laboratory team for providing technical facilities as well as substantive and equipment support, which were crucial for conducting the research described in this work. The author also wishes to express gratitude to MSc Mateusz Marek and MSc Adrian Maksymiec for their substantive assistance and for enabling the use of equipment for lens grinding.

REFERENCES

1. Christopher, J; Rooney, L M; Donnachie, M; Uttamchandani, D; McConnell, G; Bauer, R. Low-cost 3D printed lenses for brightfield and fluorescence microscopy. Biomed Opt Express 2024;15(4):2224–2237. https://doi.org/10.1364/BOE.514653
2. Du, H; Wang, Y; Li, Y; Xing, Y; Yin, S; To, S S. Fabrication of the optical lens on single-crystal germanium surfaces using the laser-assisted diamond turning. Int J Adv Manuf Technol 2024. https://doi.org/10.1007/s00170-024-13600-0
3. Sasian J. Introduction to Lens Design. Cambridge University press, 2019. 9781108625388.
4. Lupon M, Nolla C, Cardona G. New designs of spectacle lenses for the control of myopia progression: A scoping review. J Clin Med. 2024. https://doi.org/10.3390/jcm13041157
5. Todino, O F; Coppola, M; Vespini, S; Pagliarulo, V; Grilli, V; Ferraro, S. Fabrication of polymer lenses and microlens array for lab-on-a-chip devices. Opt Eng 2016;55(8):081319. https://doi.org/10.1117/1.OE.55.8.081319
6. Kozieł, G; Harasim, D; Dziuba-Kozieł, M; Kisała, P. Fourier transform usage to analyse data of polarisation plane rotation measurement with TFBG sensor. Metrol Meas Syst 2024;31(2). https://doi.org/10.24425/mms.2024.149698
7. Sun, O; Fang, F; Wang, W; Yin, J; Liu, Q; Hao, L; Peng, Y. Stereolithography 3D printing of transparent resin lens for high-power phosphor-coated WLEDs packaging. J Manuf Process 2023;85:123–134. https://doi.org/10.1016/j.jmapro.2022.11.026
8. Pillay R, Hansraj R, Rampersad N. historical development, applications and advances in materials used in spectacle lenses and contact lenses. Clin Optom (Auckl). 2020. https://doi.org/10.2147/OPTO.S257081
9. Alonso, J; Gómez-Pedrero, J A; Quiroga, J A. Modern Ophthalmic Optics. Cambridge: Cambridge University Press 2019.
10. Sommer, A C; Blumenthal, E Z. Implementations of 3D printing in ophthalmology. Graefes Arch Clin Exp Ophthalmol 2019;257:1815–1822. https://doi.org/10.1007/s00417-019-04312-3
11. Ayyildiz, O; Customised spectacles using 3-D printing technology. Clin Exp Optom 2018;101(6):747–751. https://doi.org/10.1111/cxo.12795
12. Skliutas, E; Lebedevaite, M; Kasetaite, S et al. A bio-based resin for a multi-scale optical 3D printing. Sci Rep 2020;10:9758. https://doi.org/10.1038/s41598-020-66618-1
13. Bhanvadia, A; Farley, R; Noh, Y; Toshikazu, N. High-resolution stereolithography using a static liquid constrained interface. Commun Mater 2021;2. https://doi.org/10.1038/s43246-021-00145-y
14. Mingzhe Li *et al.* Low-temperature 3D printing of transparent silica glass microstructures. Sci. Adv. 2023;9. https://doi.org/10.1126/sciadv.adi2958
15. Liam, M R; Jay, Ch; Ben, W; Yash, S; K; Copeland, L; Walker, L D; Foylan, S; William, B A; Bauer, R; McConnell, G. Printing, characterising, and assessing transparent 3D printed lenses for optical imaging. BioRxiv 2023.11.22.568002. https://doi.org/10.1101/2023.11.22.568002
16. Park, H K; Shin, M; Kim, B et al. A visible light-curable yet visible wavelength-transparent resin for stereolithography 3D printing. NPG Asia Mater 2018;10:82–89. https://doi.org/10.1038/s41427-018-0021-x
17. Grothe, T; Brockhagen, B; Storck, J L. Three-dimensional printing resin on different textile substrates using stereolithography: A proof of concept. J Eng Fibers Fabr 2020;15. https://doi.org/10.1177/1558925020933440
18. Grothe, T; Brockhagen, B; Storck, J. 3D Printing resin on different textile substrates using stereolithography: a proof of concept. J Eng Fibers Fabr 2020;15:1–7. https://doi.org/10.1177/1558925020933440
19. Ristok, S; Thiele, S; Toulouse, A; Herkommer, A H; Giessen, H. Stitching-free 3D printing of millimeter-sized highly transparent spherical and aspherical optical components. Opt Mater Express 2020;10:2370–2378.
20. Pillay, R; Hansraj, R; Rampersad, N. Historical Development, Applications and Advances in Materials Used in Spectacle Lenses and Contact Lenses. Clin Optom (Auckl) 2020 Sep 29;12:157–167. https://doi.org/10.2147/OPTO.S257081.
21. Rooney, L M; Christopher, J; Watson, B; Kumar, Y S; Copeland, L; Walker, L D; Foylan, S; Amos, W B; Bauer, R; McConnell, G. Printing, characterizing, and assessing transparent 3D printed lenses for optical imaging. Adv Mater Technol 2024. https://doi.org/10.1002/admt.202400043
22. Machado, T; Stubbs, C; Chiaradia, V; Alraddadi, M; Brandolese, A; Worch, J; Dove, A. A renewably sourced, circular photopolymer resin for additive manufacturing. Nature 2024;629:1–6. https://doi.org/10.1038/s41586-024-07399-9
23. L. M. Rooney, J. Christopher, B. Watson, Y. S. Kumar, L. Copeland, L. D. Walker, S. Foylan, W. B. Amos, R. Bauer, G. McConnell, printing, characterizing, and assessing transparent 3D printed lenses for optical imaging. Adv. Mater. Technol. 2024. https://doi.org/10.1002/admt.202400043
24. Engel, A. Progress of optical materials characterization with time. Opt Mater Express 2022;12. https://doi.org/10.1364/OME.463718A
25. Haria, R. Student to commercialize anti-epilepsy contact lenses using 3D printing; 2017. Available

from: http://www.3dprintingindustry.com/news/student-commercialize-anti-epilepsy-contact-lenses-using-3d-printing-126171/. Accessed October 2, 2019.

26. Caban, J; Szala, M; Kęsik, J; Czuba, Ł. Used of 3D printing in automotive applications. Buses – Technol Oper Transp Syst 2017. https://pub.pollub.pl/publication/82/
27. Machado, T O; Stubbs, C J; Chiaradia, V et al. A renewably sourced, circular photopolymer resin for additive manufacturing. Nature 2024;629:1069–1074. https://doi.org/10.1038/s41586-024-07399-9
28. Voet, V S D; Strating, T; Schnelting, G H M; Dijkstra, P; Tietema, M; Xu, J; Woortman, A J J; Loos, K; Jager, J; Folkersma, R. Biobased Acrylate Photocurable Resin Formulation for Stereolithography 3D Printing. ACS Omega 2018. https://doi.org/10.1021/acsomega.7b01648
29. Xu, H; Chen, S; Hu, R; Hu, M; Xu, Y; Yoon, Y; Chen, Y. Continuous vat photopolymerization for optical lens fabrication. Small 2023;19:2300517. https://doi.org/10.1002/smll.202300517
30. Wang, K; Liu, S; Chen, F; Liu, Z; Luo, X. Effect of manufacturing defects on optical performance of discontinuous freeform lenses. Opt Express 2009;17:5457–5465. https://doi.org/10.1364/OE.17.005457
31. International Organisation for Standardization. ISO 25178. Geometric Product Specifications (GPS) – Surface texture: areal 2010. Available from: https://www.iso.org/obp/ui/en/#iso:std:iso:10110:-1:ed-3:v1:en
32. Thiele, S. 3D-printed eagle eye: Compound microlens system for miniaturized high-resolution imaging. Adv Sci Technol Res J. 2025;19.
33. Ali, M et al. 3D printing of Fresnel lenses with wavelength selective tinted materials. Adv Sci Technol Res J. 2021.
34. Sani, A. Artificial intelligence-augmented additive manufacturing: Review of AI applications for 3D printing defect detection. Adv Sci Technol Res J. 2024.
35. Zhang, L; Lin, J; Shao, H; Yang, Z; Liu, B; Li, C. An unsupervised end-to-end approach to fault detection in delta 3D printers using deep support vector data description. J Manuf Syst. 2024;72.
36. Dolecki, M et al. On the Detection of Anomalies with the Use of Choquet Integral and Their Interpretability in Motion Capture Data. 2022 IEEE Int Conf Fuzzy Syst (FUZZ-IEEE), Padua, Italy; 2022:1-9. https://doi.org/10.1109/FUZZ-IEEE55066.2022.9882678
37. Powroźnik, P; Skublewska-Paszkowska, M; Dziedzic, K; Barszcz, M. Feature fusion graph consecutive-attention network for skeleton-based tennis action recognition. Appl Sci. 2025;15:5320. https://doi.org/10.3390/app15105320